Journal of Multidisciplinary Engineering Science and Technology (JMEST)
ISSN: 2458-9403
Vol. 8 Issue 8, August - 2021

Recycling of cement kiln dust as inorganic filler for ethylene-co-vinyl acetate polymer composites

Emad Mousa
Physics Department, Faculty of Science
Cairo University
Egypt
Emad@sci.cu.edu.eg

Hadeer A.Elgabry
Physics Department, Faculty of Science
Cairo University
Egypt
habdelkader@sci.cu.edu.eg

Gamal M. Nasr
Physics Department, Faculty of Science
Cairo University
Egypt
rrrrrgamal@yahoo.com

Galal H. Ramzy
Physics Department, Faculty of Science
Cairo University
Egypt
galalramzy@yahoo.com

***Abstract*—The present research studies the possibility of cement kiln dust (CKD) reuse as inorganic filler in polymer composites. The reuse of CKD as inorganic filler in polymer composites reduces both production cost and preparation efforts of fillers in polymer industry. Moreover, recycling of CKD instead of landfill disposal enhances environmental and economical sustainability for cement industry.**

The effect of CKD particles addition, without further modification, on the structural, thermal, mechanical, and electrical properties of ethylene co vinyl acetate (EVA) polymer is studied in this research.

EVA was melt-mixed in a Brabender Plasticorder with different weight proportions of CKD (0%, 1.5%, 3%, and 6%) followed by hot press. Collected CKD was characterized by X-ray fluorescence spectrometry and dynamic light scattering. The structure and physical properties of EVA/CKD composites were studied by X-ray diffraction, thermogravimetric analysis, dynamic mechanical analysis, and dielectric spectroscopy.

***The addition of CKD to EVA polymer, in the selected proportions, led to disruption of semi-crystallinity of EVA, increased thermal stability, plasticization, and increase in dielectric constant and conductivity of pure EVA*.**

Keywords— Recycling; EVA; CKD; DMA; dielectric properties

I. INTRODUCTION

Cement industry is one of the most critically important industries throughout the world [1]. But, unfortunately, cement industry has negative environmental impacts at its all stages of manufacturing. Proceeding from this, studies attempting to improve sustainability of cement industry not only concerned by improving the quality of cement products but also reported the importance of adapting raw materials supply and modifying production processes to reduce waste emissions [2]. More of that, recycling of cement by-products is crucial to reduce negative environmental impacts and to provide economic benefits such as preserving raw materials [3].

One of the main pollution sources generated from cement industry is the cement by-product dust which emitted from the raw mills, kiln system, clinker cooler, and cement mills [3], [4]. Recently, researchers succeeded to reuse cement kiln dust (CKD) in many areas of application and thus reducing its disposal by landfill [5]. Moreover, they succeeded to reclaim previously landfilled CKD to be conducted in many applications [1]. However, the recycling of CKD is evolving day by day to include; concrete and cement industry [6], glass fabrication [7], soil stabilization [8], agriculture soil enhancement [9], waste treatment [10], and formation of inorganic aluminosilicate polymer [11].

On the other hand, considering polymer industry, it is well known that the physical properties of polymer composites can be tailored to adapt the requirements of selected applications by selecting the appropriate filler. Researchers reported that fillers in the form of pure metals [12], metal salts [13], and metal oxides [14] have strong impact on the physical properties of polymer composites and thus they have long been utilized in polymer composites to suit vast fields of applications [15]. In this context, CKD could be an effortless cost saving filler in polymer industry since it consists mainly of metal salts and metal oxides.

In our present research, Ethylene-co-vinyl acetate (EVA) polymer will be used as the polymeric matrix. EVA is a flexible polymer that is commercially widely used in; hot melt adhesives, footwear and toys, water proofing, corrosion protection, and cable manufacturing. In addition, applications of EVA can be expanded to include flame retardant polymers, solar

cells, and energy saving devices by tailoring its properties via selecting the appropriate additives and methodology [16], [17].

The collected CKD will be firstly characterized by X-ray fluorescence spectrometry and dynamic light scattering. Then, the interaction between EVA matrix and CKD particles will be studied by X-ray diffraction and thermogravimetric analysis. Finally, the effect of CKD addition on the flexibility and electrical properties of EVA will be investigated through dynamic mechanical analysis and dielectric spectroscopy, respectively.

II. EXPERIMENTAL

A. Materials and Samples preparation

EVA (12% vinyl acetate) was purchased from Sigma-Aldrich Company in the form of pellets. CKD powder was supplied by Misr Beni-Suef cement Company (Beni-Suef, Egypt).

EVA was melt-mixed in a Brabender Plasticorder PLE319 (Brabender Co., Germany) at 80 °C and 80 rpm rotor speed for 5 min. Different loadings of CKD including 0%, 1.5%, 3%, and 6% (by weight) were added during the mixing process. After mixing, a constant weight (25 gm) of each sample was placed in a stainless-steel mold of dimensions 100x100x2 mm^3. All samples were pressed between the plates of an electrically hydraulic press (Model XLBD) at temperature 130 ^oC for 5 min.

B. Measurements

In order to investigate the composition of the collected CKD, elemental analysis by wavelength dispersive X-ray fluorescence spectrometry (XRF) was used [XRF, Axios advanced, sequential WD_XRF spectrometer, Malvern Panalytical Company, UK, National Research Institute]. The particle size distribution of the CKD was determined by dynamic light scattering (DLS) [ZetaSizer Nano Series (HT), Malvern Panalytical Company, UK, Egyptian Petroleum Research Institute]. The powder was dispersed in methanol at room temperature.

X-ray diffraction patterns (XRD) of pure CKD powder, pure EVA, and their composites were obtained by using an X-ray diffractometer (XRD; Empyrean, Malvern Panalytical Company, National Institute of Standards, Egypt). Measurements were performed at room temperature with Cu target Kα radiation (λ = 0.154 nm). The scanning rate was 1 deg/min ranging from 5 to 90° (2θ), with a step size of 0.013°.

Thermogravimetric (TGA) analyses of the polymer composites were carried out from room temperature to 600 °C at a rate of 10 °C/min [Shimadzu TG50H thermal analyzer, Microanalytical Center, Cairo University, Egypt].

The dynamic mechanical properties (DMA) of EVA filled CKD composites were characterized using the dynamic mechanical analyzer (Triton Instruments, Lincolnshire, UK, Egyptian Petroleum Research Institute). Rectangular specimens of 20x10x3 mm^3 were used, and the tests were performed in the tension mode at frequencies of 0.1, 0.5, 1, 5, and 10 Hz in the temperature range from -100 °C to 100 °C at a heating rate of 2 °C/min.

For electrical measurements, samples were coated with silver paste to ensure good electrical contact. The measurements were carried out using LCR-bridge (HIOKI, 3532-50 LCR HiTESTER, JAPAN) in the frequency range from 10^2 Hz up to 10^6 Hz at room temperature.

III. RESULTS AND DISCUSSION

A. Characterization of CKD

Among different elemental analysis techniques, XRF has the advantage of speed, simplicity, safety of sample preparation, and reasonable accuracy [18].

Thirteen elements namely Si, Ti, Al, Fe, Mn, Mg, Ca, Na, K, Sr, P, S and Cl have been quantified in the CKD sample by XRF technique. The concentrations of trace elements of CKD sample are presented (in percentage) in Table (1).

Table (1): Constituents of CKD as revealed by XRF

Main constituents	(wt%)
SiO_2	19.41
TiO_2	0.46
Al_2O_3	4.92
Fe_2O_3	4.35
MnO	0.12
MgO	1.21
CaO	58.60
Na_2O	0.73
K_2O	0.25
SrO	0.17
P_2O_5	0.15
SO_3	6.29
Cl	0.17
LOI	3.12
Others	0.05

It can be noticed that, Ca is the major constituent followed by Si, whereas S, Al, Fe and Mg present as minor elements, respectively. Also, the concentration of remnant elements Ti, Mn, Na, K, Sr, P, and Cl was less than 1%. Meanwhile, elements of concentrations less than 0.1% are denoted as others. Briefly, our collected CKD has high Ca content (58.60%) and low LOI value (3.12%).

Dynamic light scattering

DLS technique is distinguished by the small range of both sample volume (down to few microliters) and concentration (as low as 0.1 ppm) in addition to its high reproducibility [19]. DLS distribution analysis of tested CKD (by number %) is depicted in Fig. 1. The

figure shows two peaks; strong one (94.9 %, 28.3 nm FWHM) around 156 nm, and another weak broad peak (5.1 %, 105.4 nm FWHM) around 508 nm. In other words, most of CKD particles are less than 200 nm.

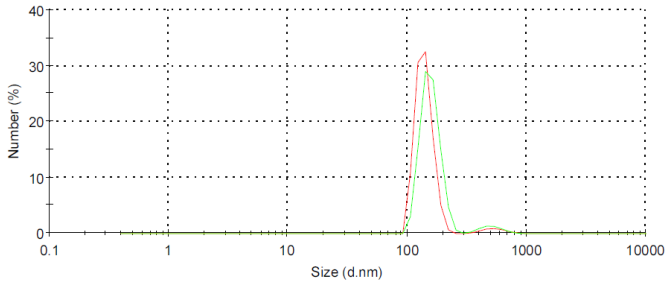

Fig. 1 Particle size distribution of CKD using DLS technique (two measurements)

B. X-ray diffraction

The XRD diffractograms of EVA copolymer and EVA/CKD composites at selected filler loadings are shown in Fig. 2. Pure EVA is characterized by its semi-crystalline nature which is controlled by the vinyl acetate (VA) content [20]. A strong crystalline peak is observed in Fig. 2 for pure EVA at 21.1°, followed by a second lower one at 23.1° [21].

As the CKD content in the EVA matrix increases, the intensity of the peak at 21.1° decreases and the peak gets broader whereas the peak at 23.1° disappears. These investigations suggest that the addition of CKD disturbs the crystalline order of the chains and increases the amorphousity of the composites.

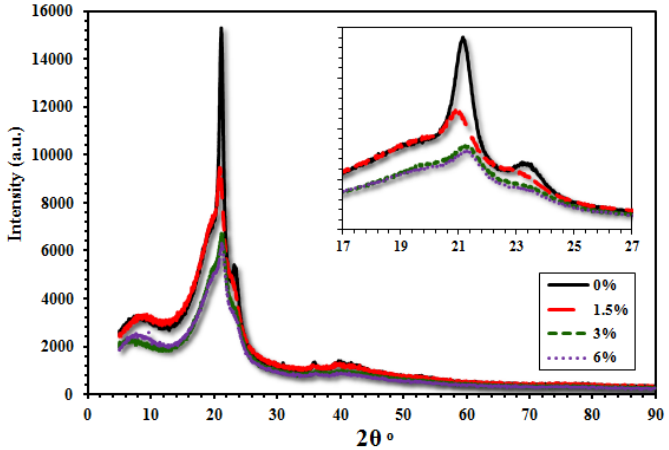

Fig. 2 XRD of pure EVA and its (1.5%, 3%, 6%) CKD loaded composites.

C. Thermogravimetric Analysis

Integral TGA thermograms of EVA composites having 0, 1.5, 3, and 6 wt% loadings of CKD are shown in Fig. 3.

Two consecutive stages of weight loss were detected in the TGA thermogram for pure EVA. The first step (305 – 352 °C) owes to the loss of acetic acid leading to the formation of poly (ethylene-co-acetylene). The second, main, decomposition step (409 – 475 °C) owes to the degradation of unsaturated polymeric chain and the evolution of butene, ethylene, methane, carbon dioxide, and carbon monoxide [22].

For EVA/CKD composites, it is obvious from Fig. 3 that the acetic acid loss in the first degradation process is catalyzed by the dispersion of CKD. A similar behavior was observed by Wilkie et al. for EVA/clay (Cloisite 30B) nanocomposites [23]. Meanwhile, the increase in CKD content shifts the decomposition temperature of the main decomposition process to higher values. Also, the temperature required to lose 50% of the sample's weight was increased, slightly, by increasing the CKD content. These results suggest higher thermal stability of EVA/CKD composites with respect to pure EVA. Finally, the residual weight of the composite samples increased with the increase in CKD content. A summary of weight losses for each process, residual weight, and $T_{50\%}$ for all samples is presented in Table (2).

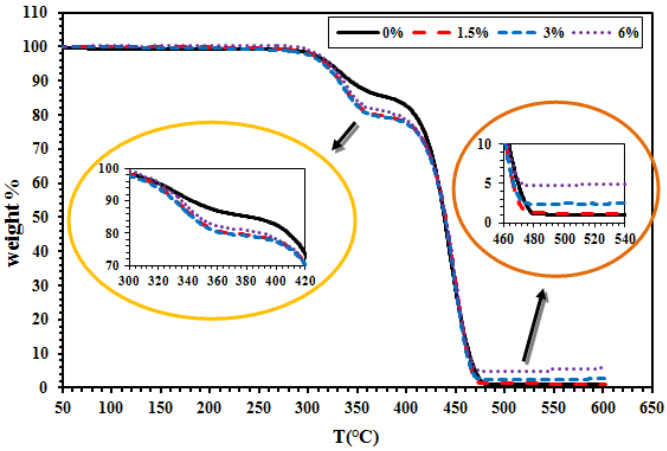

Fig. 3 Thermograms of pure EVA and its (1.5%, 3%, 6%) CKD loaded composites

A summary of weight losses for each process, residual weight, and $T_{50\%}$ for all samples is presented in Table (2)

Table (2): TGA parameters

CKD content (wt. %)	$T_{50\%}$ (^{o}C)	Residue (wt.%) at 550 ^{o}C	Decomposition steps		
			Temperature range (^{o}C)	Losses (wt.%)	E_a (kJ/mol)
0	438	0.9	305 - 352 409 - 475	12.8 81.8	97 196
1.5	440	1.1	308 - 357 410 - 477	19.1 77.6	110 206
3	439	2.9	311- 355 414 - 475	19.1 76.9	116 224
6	440	5.1	309 - 357 415 - 472	18.0 74.7	142 228

To estimate the activation energy E_a for thermal decomposition processes of EVA/CKD composites, Coats and Redfern model could be used [24]:

$$ln\left[\frac{-(1-\alpha)}{T^2}\right] = ln\left(\frac{AR}{\beta E_a}\right) - \frac{E_a}{R}\frac{1}{T} \qquad (1)$$

Where (T) is temperature in Kelvin, A is constant, β is the heating rate, R is the universal gas constant (8.314 J/mol.K), α is the fraction of degraded material, and Ea is the activation energy.

The activation energy values could be obtained from the slope of $ln\left[\frac{-(1-\alpha)}{T^2}\right]$against 1/T plots in the specified temperature range. Data were fitted to equation (1) with regression values $R^2 \geq 0.988$ and the values of E_a were summarized in Table (2). As deacetylation requires less energy than chain scission reactions, Ea values for the first decomposition step are less than those of the main decomposition step for all samples. Meanwhile, E_a increases for both decomposition processes by the increase of CKD content which may be attributed to additional partial decomposition of different CKD contents.

D. Dynamic Mechanical Analysis

DMA is a sensitive technique that can be used to study molecular relaxation processes in polymers as well as the inherent mechanical or flow properties as a function of time and temperature [25].

Effect of temperature

Fig. 4a plots the storage modulus E´ of EVA/CKD composites, obtained by DMA measurements, as a function of temperature (-100 – 100 ^{o}C) at 1 Hz.

Three regions are presented in Fig. 4a for all samples. Region (I) is the low temperature glassy region~(T < -40 ^{o}C) at which E´ is nearly independent on temperature. Meanwhile, region (II) is the glass transition region~(-40 ^{o}C < T < 40 ^{o}C) in which the material changes its state from elastic to viscous state and E´ decreases drastically with temperature. Finally, region (III) is the rubbery region ~(T > 40 ^{o}C) in which the material flows and exhibits viscous behavior with low values of E´.

At low temperatures (T ≤ -20 ^{o}C), a slight increase in E´ is observed, as shown in Fig. 4a, for EVA sample loaded with 1.5% (by weight) of CKD. Further increase in CKD content led to a subsequent decrease in E´, and consequently, in the samples' stiffness. This behavior may be understood on the basis of filler dispersion. Homogeneous filler dispersion increases the chain rigidity, resulting in an increased stiffness. At higher filler content (> 1.5%), particles tend to agglomerate. Hence, the exposed surface area of filler that interacts with polymeric chains is reduced, resulting in lower values of E´ [26]. It has been reported that crystallinity of the matrix barely affects the storage modulus at low temperature [27].

On the other hand, the presence of amorphous regions is responsible for increasing the chain mobility and decreasing the stiffness at high temperatures [27]. An observable decrease in stiffness by increasing CKD loading in all samples at temperatures (T > -20 ^{o}C), is attributed mainly to the increase in amorphous regions in accordance to XRD results.

However, relaxation processes in polymers are preferably studied in terms of loss factor (tan δ) instead of storage modulus (E´). In the glass-rubber transition region, an intense peak corresponding to the glass transition temperature (Tg) predominates the temperature dependence curve of loss factor. The intensity, broadness, and position of this peak are correlated to the structure and properties of a particular composite [28].

The temperature dependence of tan δ for EVA/CKD composites at 1 Hz is illustrated in Fig. 4b. For pure EVA curve, a damping peak exists at -18.8 ^{o}C with an extended shoulder between -10 ^{o}C and 40 ^{o}C. This shoulder belongs to the rigid amorphous portions of VA that remained rigid beyond T_g [27]. It is worth noting that this extended shoulder disappeared for all CKD loaded composites. Moreover, tan δ peak height increased with increasing CKD content as an indication of high energy damping resulting from poor interaction between inorganic CKD fillers and polymeric chains. In short, a slight decrease in T_g values may be attributed to the increase in chain mobility associated with amorphousity induced in the EVA matrix by incorporation of CKD. Values of T_g and peak height of tan δ for all samples at 1 Hz are gathered in Table (3)

Table (3): Peak height of loss factor and its corresponding peak temperature (Tg) for different EVA/CKD composites

CKD content (wt %)	(tan δ) peak height	T_g (^{o}C)
0	0.24	-18.8
1.5	0.31	-19.6
3	0.31	-20.2
6	0.32	-21.5

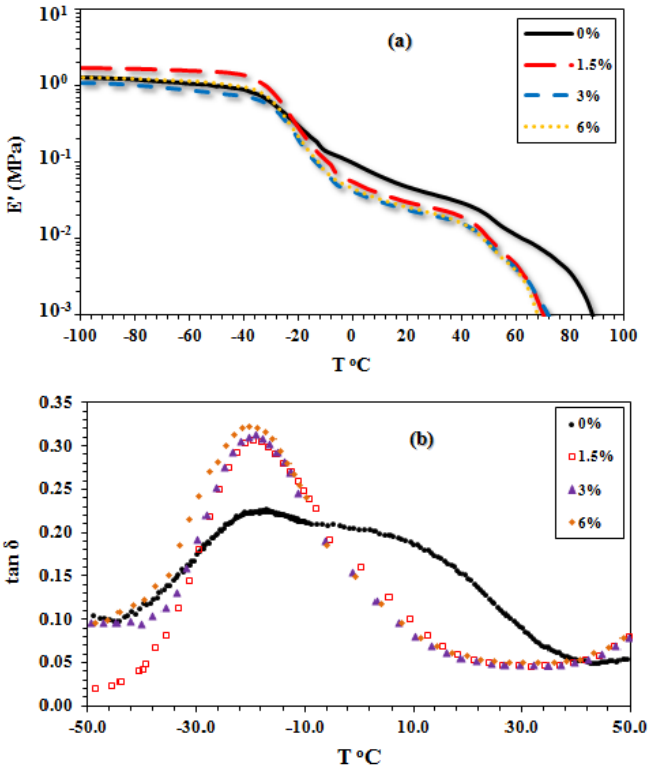

Fig. 4 Temperature dependence of a. storage modulus (E´) b. loss factor (tan δ) at 1Hz for pure EVA and its (1.5%, 3%, 6%) CKD loaded composites

Effect of frequency

In order to minimize localized stresses, a material under stress undergoes internal molecular rearrangements over a particular period of time. So, as long as the time of measurement is short (high frequency), a high measured value of elastic modulus will be resulted. Meanwhile, low frequency measurements provide enough time for the material to complete its internal rearrangements resulting in low values of elastic modulus [29].

Fig. 5a shows the frequency dependence of E´ in the viscoelastic region (-20 ^{o}C) for EVA/CKD composites. The dependence of for E´(ω) for EVA/CKD composites may be expressed in the form [30]:

$$E'(\omega) \alpha \omega^{n} \quad (2)$$

where (ω=2πf) is the angular frequency (rad/S) and (n) is a dimensionless power factor. Values of n are summarized in Table (4).

It was reported that T_g depends strongly on the rate of measurement (frequency/temperature) [31]. Accordingly, T_g increases with frequency as a dephasing response of composites at high frequencies, and Arrhenius equation is used to express the frequency dependence of T_g [32]:

$$lnf = lnf_o - \frac{\Delta E_a}{R}\frac{1}{T_g} \quad (3)$$

where (f) is the frequency of measurement, (T_g) is the glass transition temperature deduced from loss factor peak temperature and expressed in (Kelvin), (R=8.341 J/mol.K) general gas constant, and (ΔE_a) is the activation energy of glass transition.

Table (4): The power factor of equation (2) and the activation energy of transition (ΔE_a) with their relevant regression factors (R^2)

CKD content (wt %)	n at -20 °C	R^2	ΔE_a (kJ/mole)	R^2
0	0.129	0.999	403	0.996
1.5	0.173	0.998	382	0.995
3	0.188	0.999	368	0.998
6	0.176	0.998	355	0.991

The activation energy of glass transition represents the energy required to initiate segmental mobility of polymeric chains. (ΔE_a) values for all samples are calculated in Table (4) from the slope of (lnf) vs (1000/T) plots as presented in Fig. 5b

It can be concluded from Table (4) that a considerable decrease in the activation energy is associated with the increase of CKD content in EVA/CKD composites. The increased amorphousity in the EVA matrix upon loading CKD particles alongside the presence of more free space for molecular vibration due to the aggregation of filler particles that caused enlargement of intersegment distances are responsible for the low values of ΔE_a. However, this plasticization effect of CKD particles to the EVA matrix can be inverted to induce reinforcement instead, for selected applications, by appropriate modifications at the EVA/CKD interface

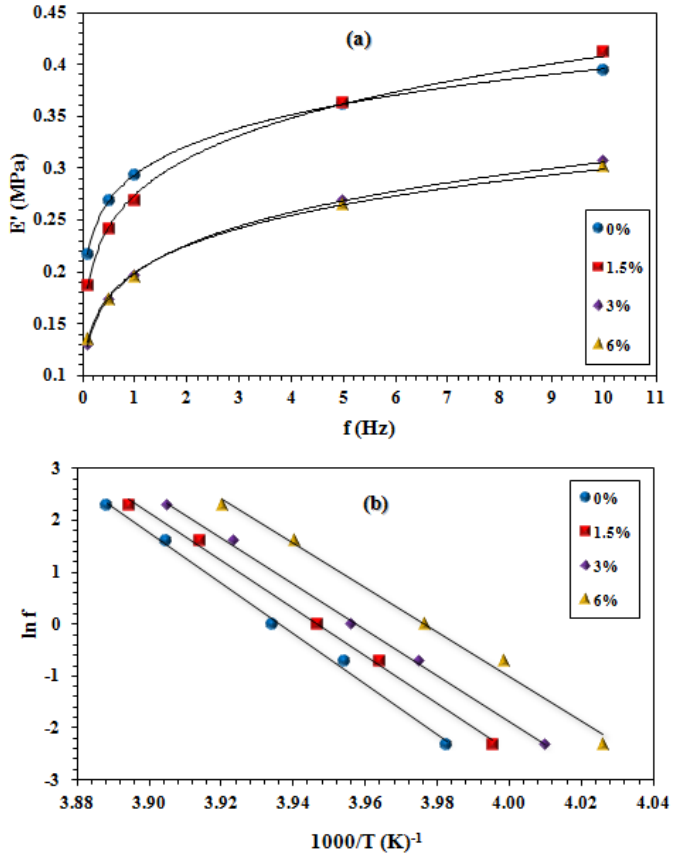

Fig. 5 a. Frequency dependence of storage modulus (E´) at -20 ^{o}C for different EVA/CKD composites, and solid lines represent theoretical fitting to equation (2) b. Arrhenius plot of (ln f) versus ($1000/T_g$) for different EVA/CKD composites, and solid lines represent theoretical fitting to equation (3)

E. Dielectric Properties

A valuable experimental tool for understanding the phenomena of charge transport in polymers is dielectric spectroscopy [33]. Fig. 6a illustrates the frequency dependence of the real part of the dielectric constant (ε′) for all samples at room temperature. Although ε′ increases at all frequencies with increasing CKD loading in EVA matrix, all composites are still considered low dielectric materials. The dispersion of CKD particles in the dielectric EVA matrix led to the formation of micro capacitor network which increased by increasing the CKD content [34]. A frequency independent behavior of ε′ for pure EVA is observed up to 10^4 Hz as a consequence of β-relaxation resulting from acetate side chains movement [35]. Regardless of limited dispersion arising from interfacial polarization at low frequency, ε′ for CKD loaded samples showed a plateau up to 10^4 Hz similar to that observed for pure EVA. However, the weak frequency dependence of ε′ for EVA/CKD composites may be crucial for practice applications [36].

On the other hand, the frequency dependence of dielectric loss (ε″) for all samples at room temperature is presented in Fig. 6b. An observed increase in ε″ with the increase in CKD loading, at all frequencies, is attributed to distortional dipolar, interfacial, and conduction losses [37]. Furthermore, ε″ spectra for all samples showed a negative slope (up to 200 Hz) followed by a frequency independent region (up to 6 kHz), and then ε″ continues to increase. The negative slopes indicate that DC conductivity and/or universal dynamic response (UDR) of conductivity are predominant in this frequency range according to Jonscher [38]:

$$\sigma \alpha \omega^{S}, \qquad 0 < S < 1 \tag{4}$$

where ε″ at a particular temperature and certain angular frequency (ω) is related to the AC conductivity (σ) by the relation:

$$\sigma = \varepsilon_0 \omega \varepsilon'' \tag{5}$$

and S is a power factor that may be correlated to the conduction mechanism according to its frequency and temperature behavior.

Meanwhile, the frequency-independent region of ε″ in Fig. 6b is known as the nearly constant loss (NCL) regime which implies a linear frequency dependence of conductivity [39]:

$$\sigma \propto \omega^{S}, \qquad S = 1 \tag{6}$$

Finally, the positive slopes of ε″ appeared toward the high-frequency end demonstrate a change from the well known Jonscher's power law to a superlinear power law (SPL) as suggested by Lunkenheimer and Loidl [40]:

$$\sigma \propto \omega^{S}, \qquad S > 1 \tag{7}$$

The sublinear behavior (S < 1) is very common in glassy and crystalline ionic solids along with semi-conducting solids [41], whereas linear (S = 1) and superlinear behaviors (S > 1) have also been found in poorly conducting oxide glasses [39], superionic conductor glasses [42], Schiff base metal complexes [43], and ferroelectric ceramics [44].

Fig. 6c represents the frequency dependence of conductivity for EVA/CKD composites at room temperature. Obviously, the conductivity of EVA matrix increases slightly by increasing the CKD loading as the amount of metal oxides/salts constituting CKD particles increases. However, a DC plateau exists in all samples at low frequency followed by an increase in conductivity upon increase of frequency, and the frequency behavior in Fig. 6c can be fitted to a modified Jonscher equation [41]:

$$\sigma_{(\omega)} = \sigma_{DC} + A\omega^{S_1} + B\omega^{S_2} \tag{8}$$

where $\sigma_{\_DC}$ is the DC conductivity, $0 < S_1 < 1$ accounts for UDR and dominates at low frequencies and corresponds to translational motion, $1 \leq S_2 < 2$ accounts for NCL/SPL and dominates at high frequencies and corresponds to reorientational motion, and A and B are thermally activated parameters. The fitting parameters to equation (8) are summarized in Table (5).

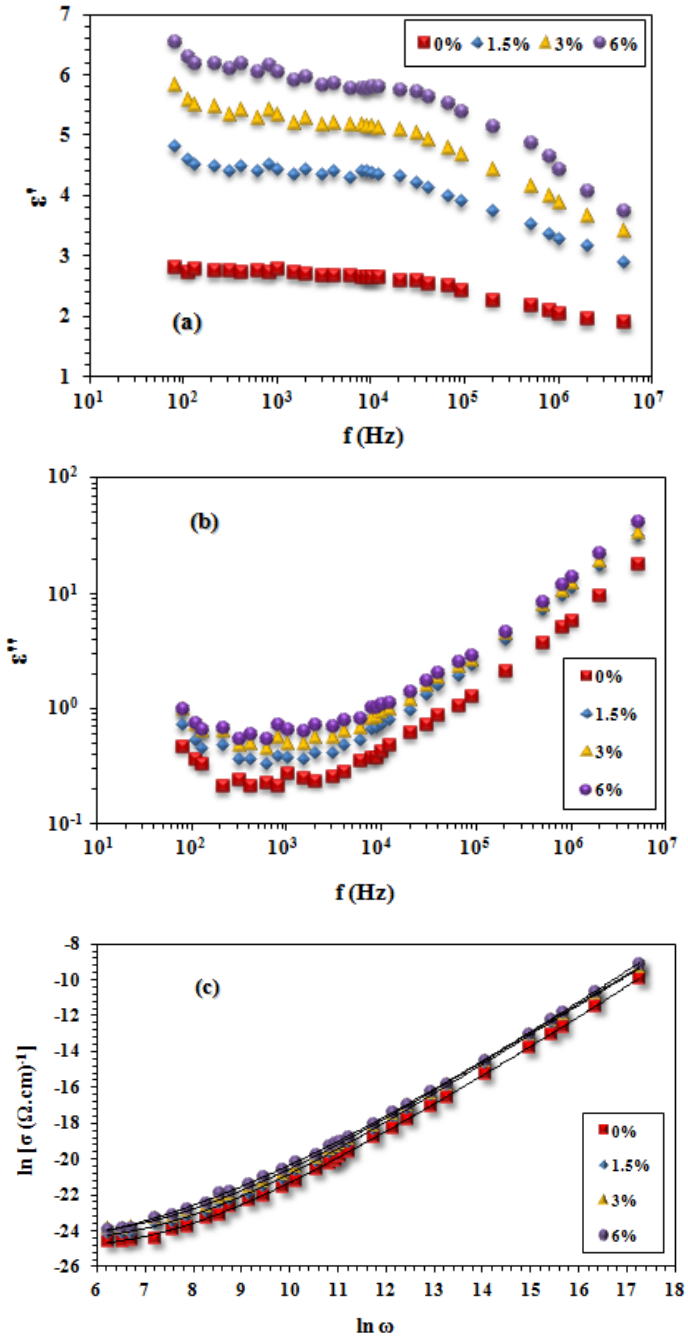

Fig. 6 Frequency dependence of a. dielectric constant (ε′) b. dielectric loss (ε″) c. AC conductivity (σ_{AC}) for pure EVA and its (1.5%, 3%, 6%) CKD loaded composites. Solid lines represent theoretical fitting to equation (8)

Table (5): Fitting parameters to equation (8)

CKD content (wt %)	σ_{DC} $(\Omega.cm)^{-1}$	A	S_1	B	S_2	R^2
0	$1.16*10^{-11}$	$1.35*10^{-14}$	0.98	$1.69*10^{-17}$	1.66	0.998
1.5	$1.53*10^{-11}$	$5.73*10^{-14}$	0.87	$3.74*10^{-17}$	1.65	0.999
3	$2.43*10^{-11}$	$2.91*10^{-14}$	0.91	$2.29*10^{-17}$	1.69	0.999
6	$2.92*10^{-11}$	$3.79*10^{-14}$	0.97	$4.98*10^{-17}$	1.64	0.998

CONCLUSION

In conclusion, reuse of CKD as inorganic filler for EVA polymer composites is examined in this work for the first time. Characterization of used CKD particles by XRF and DLS revealed that Ca is the main constituent element, and most of CKD particle size is less than 200 nm. EVA/CKD composites with different weight proportions of CKD (0%, 1.5%, 3%, 6%) were successfully prepared by melt mixing followed by hot press. Structural analysis of prepared composites by XRD concluded that semi-crystalline nature of EVA is disrupted by CKD addition. Meanwhile, TGA measurements showed that all samples are thermally stable up to 300 ^{o}C, and the decomposition temperature increases by addition of CKD. Results of DMA recorded an increased stiffness at the glassy region for 1.5% loaded CKD sample, as indication of well dispersion. Whereas a decrease in T_g values and their associated activation energies alongside an observable decrease in stiffness beyond the glassy region reflects plasticization effect of EVA by addition of CKD due to increased amorphousity. Dielectric studies demonstrate a frequency independent behavior of ε′ for all samples up to 10^4 Hz. The AC conductivity of all samples showed a cross-over from the UDR response to the SPL.

References

[1] W. S. Adaska, D. H. Taubert, and others, “Beneficial uses of cement kiln dust,” in 2008 IEEE Cement Industry Technical Conference Record, 2008, pp. 210–228.

[2] J. H. Potgieter, “An Overview of Cement production: How ‘green’ and sustainable is the industry?,” Environ. Manag. Sustain. Dev., vol. 1, no. 2, pp. 14–37, 2012.

[3] A. A. Elbaz, A. M. Aboulfotoh, A. M. Dohdoh, and A. M. Wahba, “Review of beneficial uses of cement kiln dust (CKD), fly ash (FA) and their mixture,” J. Mater. Environ. Sci., vol. 10, no. 11, pp. 1062–1073, 2019.

[4] S. M. El Haggar, “Rural and Developing Country Solutions,” in Environmental Solutions, F. J. Agardy and N. L. Nemerow, Eds. Burlington: Academic Press, 2005, pp. 313–400.

[5] R. Siddique, “Cement Kiln Dust,” in Waste Materials and By-Products in Concrete, Berlin, Heidelberg: Springer Berlin Heidelberg, 2008, pp. 351–380.

[6] A. Sreekrishnavilasam, S. King, and M. Santagata, “Characterization of fresh and landfilled cement kiln dust for reuse in construction applications,” Eng. Geol., vol. 85, no. 1–2, pp. 165–173, May 2006.

[7] B. Hamann, M. Schulz, C. Schneider, I.-B. GlasPartner, and V. V Deutscher Zementwerke, “Use of alkaline process dusts from the cement industry in glass production processes,” Veröffentlichung_DGG-Journal, no. July, 2008.

[8] N. L. Hussey, A. B. Cerato, J. G. Grasmick, E. S. Holderby, G. A. Miller, and W. Tabet, “An Assessment of Soil Parameters Governing Soil Strength Increases with Chemical Additives,” in GeoFlorida 2010: Advanced in Analysis, Modeling & Design, 2010, pp. 2702–2711.

[9] M. Francis, Background Report on Fertilizer Use, Contaminants and Regulators. DIANE Publishing, 2000.

[10] A. H. Mostafa, “Effect of cement kiln dust addition on activated sludge process without primary settling for reuse applications,” HBRC J., vol. 8, no. 1, pp. 14–25, Apr. 2012.

[11] D. Kubatová, A. Rybová, A. Zezulová, and J. Švec, “Thermal behaviour of inorganic aluminosilicate polymer based on cement kiln dust,” IOP Conf. Ser. Mater. Sci. Eng., vol. 379, no. 1, 2018.

[12] I. Krupa, V. Cecen, A. Boudenne, J. Prokeš, and I. Novák, “The mechanical and adhesive properties of electrically and thermally conductive polymeric composites based on high density polyethylene filled with nickel powder,” Mater. Des., vol. 51, pp. 620–628, 2013.

[13] F. K. M. Genova, S. Selvasekarapandian, S. Karthikeyan, N. Vijaya, R. Pradeepa, and S. Sivadevi, “Study on blend polymer (PVA-PAN) doped with lithium bromide,” Polym. Sci. - Ser. A, vol. 57, no. 6, pp. 851–862, 2015.

[14] A. Hassena, S. El-Sayeda, W. M. Morsic, and A. M. El Sayedb, “PREPARATION, DIELECTRIC AND OPTICAL PROPERTIES OF Cr2O3 /PVC NANOCOMPOSITE FILMS,” J. Adv. Phys., vol. 4, no. 3, pp. 571–584, 2014.

[15] G. Wypych, Handbook of Fillers, vol. 28, no. 2. 1999.

[16] H. W. Di, C. Deng, R. M. Li, L. P. Dong, and Y. Z. Wang, “A novel EVA composite with simultaneous flame retardation and ceramifiable capacity,” RSC Adv., vol. 5, no. 63, pp. 51248–51257, 2015.

[17] D. priyadarsini Jena, B. Mohanty, R. K. Parida, B. N. Parida, and N. C. Nayak, “Dielectric and thermal behavior of 0.75BiFeO3-0.25BaTiO3 filled ethylene vinyl acetate composites,” Mater. Chem. Phys., vol. 243, no. November 2019, p. 122527, 2020, doi: 10.1016/j.matchemphys.2019.122527.

[18] A. Y. Ahmed, M. P. Abdullah, A. K. Wood, M. S. Hamza, and M. R. Othman, “Determination of some trace elements in marine sediment using ICP-MS and XRF (a comparative study),” Orient J Chem, vol. 29, no. 2, pp. 645–653, 2013.

[19] S. K. Brar and M. Verma, “Measurement of nanoparticles by light-scattering techniques,” TrAC - Trends Anal. Chem., vol. 30, no. 1, pp. 4–17.

[20] M. Brogly, M. Nardin, and J. Schultz, “Effect of vinylacetate content on crystallinity and second-order transitions in ethylene-vinylacetate copolymers,” J. Appl. Polym. Sci., vol. 64, no. 10, pp. 1903–1912.

[21] T. Kuila, P. Khanra, A. K. Mishra, N. H. Kim, and J. H. Lee, “Functionalized-graphene/ethylene vinyl acetate co-polymer composites for improved mechanical and thermal properties,” Polym. Test., vol. 31, no. 2, pp. 282–289, 2012.

[22] M. B. Maurin, L. W. Dittert, and A. A. Hussain, “Thermogravimetric analysis of ethylene-vinyl acetate copolymers with Fourier transform infrared analysis of the pyrolysis products,” Thermochim. Acta, vol. 186, no. 1, pp. 97–102, 1991.

[23] M. C. Costache, D. D. Jiang, and C. A. Wilkie, “Thermal degradation of ethylene--vinyl acetate coplymer nanocomposites,” Polymer (Guildf)., vol. 46, no. 18, pp. 6947–6958, 2005.

[24] E. Mousa, Y. Hafez, and G. M. Nasr, “Optical Study on PVA/PEG Blend Doped with Nano-Silica,” J. Electron. Mater., vol. 50, no. 5, pp. 2594–2604.

[25] J. D. Menczel and R. B. Prime, “Thermal Analysis of Polymers: Fundamentals and Applications,” Therm. Anal. Polym. Fundam. Appl., pp. 1–688, 2008.

[26] T. E. Motaung, A. S. Luyt, M. L. Saladino, D. C. Martino, and E. Caponetti, “Morphology, mechanical properties and thermal degradation kinetics of PMMA-zirconia nanocomposites prepared by melt compounding,” Express Polym. Lett., vol. 6, no. 11, pp. 871–881, 2012.

[27] Y. T. Sung, C. K. Kum, H. S. Lee, J. S. Kim, H. G. Yoon, and W. N. Kim, “Effects of crystallinity and crosslinking on the thermal and rheological properties of ethylene vinyl acetate copolymer,” Polymer (Guildf)., vol. 46, no. 25, pp. 11844–11848, 2005.

[28] H. L. Ornaghi, A. S. Bolner, R. Fiorio, A. J. Zattera, and S. C. Amico, “Mechanical and dynamic mechanical analysis of hybrid composites molded by resin transfer molding,” J. Appl. Polym. Sci., vol. 118, no. 2, pp. 887–896, 2010.

[29] L. A. Pothan, S. Thomas, and G. Groeninckx, “The role of fibre/matrix interactions on the dynamic mechanical properties of chemically modified banana fibre/polyester composites,” Compos. Part A Appl. Sci. Manuf., vol. 37, no. 9, pp. 1260–1269, Sep. 2006.

[30] M. Abu-Abdeen, “Static and dynamic mechanical properties of poly(vinyl chloride) loaded with aluminum oxide nanopowder,” Mater. Des., vol. 33, no. 1, pp. 523–528, 2012.

[31] M. R. Aghjeh, H. A. Khonakdar, and S. H. Jafari, “Application of mean-field theory in PP/EVA blends by focusing on dynamic mechanical properties in correlation with miscibility analysis,” Compos. Part B Eng., vol. 79, pp. 74–82, May 2015.

[32] W. Stark and M. Jaunich, “Investigation of Ethylene/Vinyl Acetate Copolymer (EVA) by thermal analysis DSC and DMA,” Polym. Test., vol. 30, no. 2, pp. 236–242, Apr. 2011.

[33] G. M. Nasr and R. M. Ahmed, “AC CONDUCTIVITY AND DIELECTRIC PROPERTIES OF PMMA/FULLERENE COMPOSITES,” Mod. Phys. Lett. B, vol. 24, no. 9, pp. 911–919, 2010.

[34] S. Choudhary and R. J. Sengwa, “Anomalous dielectric behaviour of poly(vinyl alcohol)-silicon dioxide (PVA-SiO2) nanocomposites,” AIP Conf. Proc., vol. 1728, 2016.

[35] S. Hui, T. K. Chaki, and S. Chattopadhyay, “Dielectric properties of EVA/LDPE TPE system: Effect of nanosilica and controlled irradiation,” Polym. Eng. Sci., vol. 50, no. 4, pp. 730–738, 2010.

[36] Z. M. Dang, J. K. Yuan, J. W. Zha, T. Zhou, S. T. Li, and G. H. Hu, “Fundamentals, processes and applications of high-permittivity polymer-matrix composites,” Prog. Mater. Sci., vol. 57, no. 4, pp. 660–723.

[37] M. K. Mohanapriya, K. Deshmukh, B. Ahamed, K. Chidambaram, and S. Pasha, “Zeolite 4A Filled Poly (3, 4-Ethylenedioxythiophene): (Polystyrenesulfonate) (PEDOT: PSS) And Polyvinyl Alcohol (PVA) Blend Nanocomposites As High-K Dielectric Materials For Embedded Capacitor Applications,” Adv. Mater. Lett., vol. 7, pp. 996–1002, 2016.

[38] A. K. Jonscher, “Dielectric relaxation in solids,” J. Phys. D. Appl. Phys., vol. 32, no. 14, p. R57, 1999.

[39] A. S. Nowick, A. V Vaysleyb, and W. Liu, “Identification of distinctive regimes of behaviour in the ac electrical response of glasses,” Solid State Ionics, vol. 105, no. 1–4, pp. 121–128, 1998.

[40] P. Lunkenheimer and A. Loidl, “Response of Disordered Matter to Electromagnetic Fields,” Phys. Rev. Lett., vol. 91, no. 20, p. 207601, Nov. 2003.

[41] J. P. Tiwari and K. Shahi, “Super-linear frequency dependence of ac conductivity of disordered Ag2S–Sb2S3 at cryogenic temperatures,” Philos. Mag., vol. 87, no. 29, pp. 4475–4500, 2007.

[42] D. P. Singh, K. Shahi, and K. K. Kar, “Superlinear frequency dependence of AC conductivity and its scaling behavior in xAgI-(1- x) AgPO3 glass superionic conductors,” Solid State Ionics, vol. 287, pp. 89–96, 2016.

[43] E. S. Mousa and W. H. Mahmoud, “Spectroscopic, textural, electrical and magnetic properties of antimicrobial nano Fe (III) Schiff base complex,” Appl. Organomet. Chem., vol. 33, no. 6, p. e4844, 2019.

[44] S. Ke, H. Huang, S. Yu, and L. Zhou, “Crossover from a nearly constant loss to a superlinear power-law behavior in Mn-doped Bi (Mg1/2 Ti1/2) O3 - PbTiO 3 ferroelectrics,” J. Appl. Phys., vol. 107, no. 8, pp. 13–17.